Nanoscale Oxygen Generators: MgO_2-Based Fillings of BN Nanotubes

Dmitri Golberg,* Yoshio Bando, Keita Fushimi, Masanori Mitome, Laure Bourgeois,† and Cheng-Chun Tang

Advanced Materials Laboratory and Nanomaterials Laboratory, National Institute for Materials Science, Namiki 1-1, Tsukuba, Ibaraki 305-0044, Japan

Received: March 28, 2003; In Final Form: June 23, 2003

Boron nitride (BN) nanotubes having only tens of nanometers in diameter and open tip-ends were uniformly filled with a MgO_2-based material. The crystal structures and chemical compositions of the tubes and filling media were analyzed using high-resolution and energy-filtered electron microscopy, electron diffraction, electron energy loss, and energy dispersion X-ray spectroscopy. A low melting point (∼88 °C) and easy decomposition of the filling inside the tubes under moderate heating, e.g., during in-situ electron irradiation in an electron microscope, and/or just during room temperature aging, may generate a spatially localized oxygen outflow from the nanotubes. The MgO_2-filled material is uniquely characterized by a stable oxygen release rate with long release term. Thus the first nanotube-based oxygen generator has been realized.

Utilizing nanotubes[1] as ultimate ultralight gas containers has attracted major interest with respect to practical applications.[2−5] Hydrogen and nitrogen were observed to penetrate, remain inside, and be easily released from C nanotubes.[2−5] However, the possibility of using nanotubes as localized oxygen burners and/or generators has not yet been investigated. In addition, gaseous oxygen is expected to quickly damage the interior of a C nanotubular structure via fast oxidation at relatively moderate temperatures (∼500−600 °C), making a C nanotube-based oxygen container probably unfeasible. A boron nitride (BN) nanotube[6,7] is the counterpart of a C nanotube in which alternating B and N atoms entirely substitute for C atoms in a honeycomb network. The BN tubes have been found to be much more stable to oxidation in air by revealing an excellent thermal and chemical stability.[8]

Magnesium forms several oxides, e.g., MgO, MgO_2, and MgO_4.[9,10] The last oxide is highly unstable at atmospheric pressure and temperatures just above ∼30 °C. A hypothetical Mg_2O phase has also been considered.[10] MgO is one of the most stable inorganic compounds with a melting point of ∼2800 °C. By contrast, MgO_2 is an unstable material exhibiting melting at just ∼88 °C, followed by gradual decomposition, which, in turn, generates oxygen. An ab initio quantum mechanical study has displayed that peroxide MgO_2 is energetically unstable, having a decomposition reaction energy of −26.8 kJ/mol, and that the presence of water and/or hydrogen peroxide may be necessary for stabilization of the structure.[11] In fact, pure MgO_2 was shown to be prone to self-ignition in air.[12]

In practice, it has been observed that MgO_2 films may form on conventional MgO materials during heating.[13] It has been found that, compared to other peroxides, MgO_2 can generate O_2 gas during a relatively long period of time.[14,15] For example, concrete briquets used in a permeable barrier system for the groundwater flow and containing 21 wt % MgO_2, released oxygen at measurable rates for up to 300 days.[15] MgO_2 was suggested as the best possible candidate for use in saturated surface soil applications due to its lowest oxygen release rate among other soil chemical amendments.[16] Moreover, an oxygen release compound based on MgO_2 was found to be efficient in the decontamination of ground soils from petroleum traces[17] and restoration of normal glucose and cholesterol levels in a human body.[18]

The present Letter describes the synthesis and analysis of pure open-ended BN nanotubes, only tens of nanometers in diameter, filled with a MgO_2-based material that may easily decompose inside the tubes and thus locally generate oxygen when subjected to marginal heating, as for example, by an electron beam, and/or just during room-temperature aging. Thus the first nanoscale oxygen burner or generator has been created.

A mixture of B and MgO (with molar ratio of 1:1) was placed in a BN crucible and heated to 1300 °C using a high-frequency (21.5 MHz) induction furnace.[19] At this temperature B reacted with MgO to form B_2O_2 and Mg vapors.[20] The vapors were transported with the aid of an Ar flow into a reaction chamber whose temperature was preliminarily set to ∼1550 °C, with subsequent introduction of a flow of NH_3. A BN material crystallized on a Mo substrate located in the upper zone of the chamber through a simple chemical reaction between B_2O_2 and NH_3. The involved chemical reactions are written as follows:[19]

$$2B(s) + 2MgO(s) \rightarrow B_2O_2(g) + 2Mg(g) \quad (1)$$

$$B_2O_2(g) + 2NH_3(g) \rightarrow 2BN(s) + 2H_2O(g) + H_2(g) \quad (2)$$

After complete evaporation of the reagents and subsequent cooling to room temperature over 2 h, a bright-grey product was obtained at the Mo substrate.

The resultant product was analyzed using high-resolution transmission electron microscopes JEOL-3000F and JEOL-3100FEF, both operated at 300 kV. The former microscope was equipped with a Gatan 766 electron energy loss (EELS) spectrometer and an X-ray energy dispersion (EDS) detector, whereas the latter microscope was equipped with an energy filter (Omega-type), making possible elemental mappings along with

* To whom correspondence should be addressed. E-mail: golberg.dmitri@nims.go.jp.

† Permanent address: School of Physics and Materials Engineering, P.O. Box 69M, Monash University, Victoria 3800, Australia.

10.1021/jp030383y CCC: $25.00
Published on Web 08/02/2003

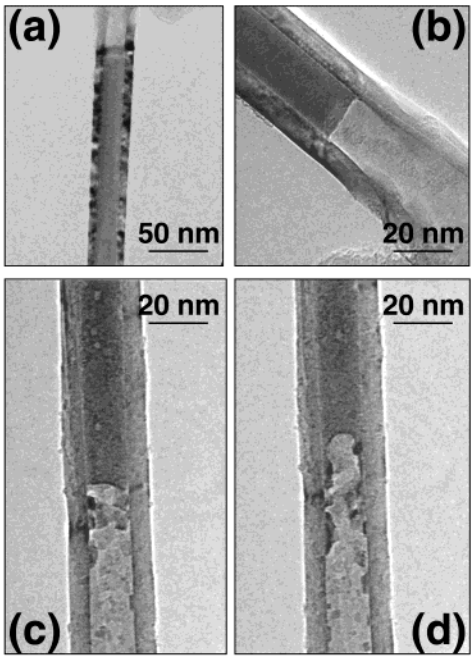

Figure 1. Representative transmission electron microscope (TEM) images of the filled nanotubes (a−d) found in the resultant synthesis product. Low-magnification TEM image (a) and an image clearly displaying a filled tube/empty tube boundary (b). Electron beam irradiation-induced changes within the filling [(c) and (d)], beam intensity ∼60 pA/cm^2: initial irradiation, e.g., 1−2 min (c); longer irradiation, e.g., 3−5 min (d).

structural and electron diffraction studies. A three window procedure was utilized for elemental map recording (two preedge and one postedge energy-filtered images were taken). The exposure time was set at 10, 12, 15, 18, and 20 s for B, C, N, O, and Mg map acquisitions, respectively. The microscope magnification was adjusted to 15 × 10^4 during mapping. EEL spectra quantification was performed using hydrogenic cross-sections. Absolute edge energies were calibrated using the graphitic π^* B peak at 188 eV.

Figure 1a−d depicts representative filled nanotubes found in the product. Nanotubes were approximately 20−100 nm in diameter and several micrometers in length. They displayed solely open tip-ends. The yield of filled nanotubes, as compared to that of unfilled ones, was estimated as ∼50 vol %. It is striking that the present utilization of a refractory metal template (Mo) for the nanotube crystallization and increase in the furnace temperature from 1300 °C (used in the previous synthesis of unfilled pure BN nanotubes using the similar experimental setup)[19] to 1550 °C was found to be crucial for obtaining filled tubes, albeit the reason behind this phenomenon has not been well-understood.

During an initial microscopic study, we immediately noted that the filling material was easily melted and evaporated from inside the tubes during conventional TEM operations. Parts c and d of Figure 1 display two consecutive HRTEM images of a filled tube subjected to irradiation with a ∼60 pA/cm^2 electron beam current density over several minutes. Evaporation and fragmentation of the filling is obvious in both figures.

The chemical composition of the nanotubes and their fillings was analyzed using EELS and EDS. The data are respectively shown in Figure 2a−c. Only the B and N K-edges are detected in the EEL spectrum, Figure 2b (black), taken on the hollow nanotube part encircled in Figure 2a. Quantification of the EEL spectrum gives a B/N ratio of ∼1.08 ± 0.15 (the error arises due to insurmountable uncertainty in background subtraction).

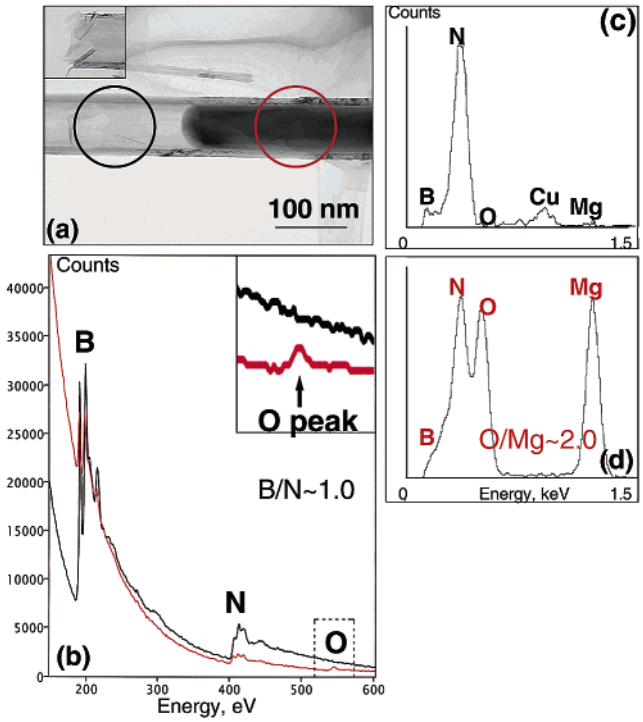

Figure 2. Results of filled nanotube chemical characterization. TEM image of a half-filled nanotube with two encircled domains; in black (hollow tube) and in red (filled tube) (a). The inset highlights a typically open-tube tip-end. (b) Comparative EEL spectra recorded from a hollow tube part (black line) and a filled tube part (red line); the inset depicts an enlarged portion of a O core-loss K-edge located at 532 eV. Position of the B (188 eV) and N (401 eV) core-loss K-edges and a calculated B/N atomic ratio are also shown. (c), (d) Comparative ED spectra taken from a hollow tube part [peaks marked in black in (c)] and a filled tube part [peaks marked in red in (d)]. A calculated atomic O/Mg ratio of ∼2.0, consistent with a MgO_2 formula, is marked in the lower ED spectrum. A Cu signal in the upper ED spectrum in (c) originates from the supporting Cu TEM grid, whereas all other reflections come from either exclusively BN shielding layers (c) or superimposed from a BN tubular shield and a MgO_2–based core filling (d).

Thus the tube is made of pure BN tubular shells. By contrast, an EEL spectrum, Figure 2b (red), taken on a filled tube part, also encircled in Figure 2a, while still exhibiting analogous B and N edges, in addition, displays a notable O peak, obviously originating from the tube filling. Quantification of the "red" EEL spectrum, Figure 2b, again gives a B/N ratio of ∼1.09 ± 0.15, but an O/B ratio of 0.46 ± 0.07. This implies (i) the B and N signals solely originate from the shielding BN tubular walls rather than being overlapped from the tube and the filling and (ii) O is present in the filling. An ED spectrum, Figure 2c, taken on the unfilled nanotube part reveals only B, N, and Cu signals. The Cu one originates from the supporting TEM grid. No other notable peaks are seen in the spectrum. However, strong Mg and O X-ray peaks, along with the familiar B and N peaks (originating from the shielding stoichiometric BN tubular layers), appeared in the ED spectrum, Figure 2d, taken from the filled nanotube part using a ∼5.7 pA/cm^2 electron beam current density over a limited exposure time (3 s). Quantification of this ED spectrum gives a O/Mg ratio of ∼2.0, i.e., the MgO_2 formula. Thus, generally, the chemical composition of the filling might be suggested to be close to a stoichiometric MgO_2. We would not fully rule out the presence of doping species, i.e., B, C, and N, readily available during the high-temperature synthesis, in the filled MgO_2 phase at a level not detectable by our analysis means. It is also noted that ∼0−12 at. % of a Si impurity, originating from the quartz tube and crucible used,

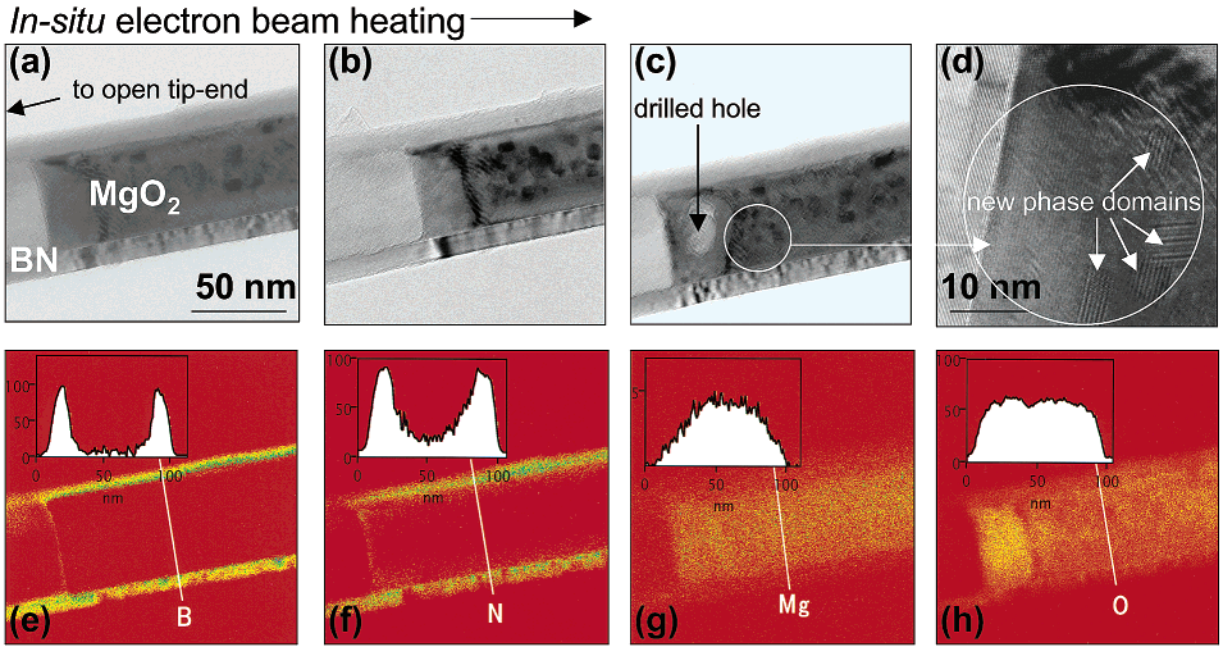

Figure 3. Transmission electron microscopy (TEM) images (a−d) and energy-filtered elemental maps (e−h) of a representative MgO_2-based-filled BN nanotube. Electron beam irradiation heating with a beam intensity of ~18 pA/cm^2 over 10 min was performed from (a) to (c). A fragment of the filling close to a drilled hole (depicted with an arrow) in (c) is enlarged in (d) to clearly display the nature of the numerous dark-contrast areas appearing under heating. This was assigned to precipitates of a stable Mg-containing phase (e.g., Mg-based solid solution), marked with the arrows in (d). The B (e), N (f), Mg (g), and O (h) elemental maps were constructed at some intermediate irradiation stage well before the irradiation-induced hole appearance in (c). Each element composition profile across the filled tube (along the cross-sectional lines marked in white) is attached to the corresponding elemental map in (e−h) as an inset.

was sometimes observed within the MgO_2-based fillings during numerous EDS runs undertaken. We also suggest that the H_2O and H_2 molecules forming via the reaction 2 may stabilize a MgO_2-based lattice during cooling, in line with the theoretical and experimental facts available in the literature.[11,12]

No detailed diagram for the Mg−O system has been published. The schematically assessed diagram is available for the range 0−50 at. % O only.[10] At low temperatures Mg at its O-rich limit is considered to be in equilibrium with MgO_2, which is stable in a range of O_2 fugacities greater than those at which MgO is stable.[10] Most likely, the present MgO_2-based fillings are formed during cooling Mg- and/or MgO-based-filled BN nanotubes (frequently observed by TEM and EDS in the specimens) to room temperature in an oxygen-containing environment with a high partial oxygen pressure (probably experienced by some Mg-containing nanotube cores). For instance, Mg may be oxidized to MgO_2 below ~230 °C ($\Delta H°_{f298}$ = 623 kJ/mol).[9]

Figure 3a−h depicts a sequence of MgO_2-based-filled open-ended BN tube transformations under in situ electron irradiation with a beam current density ~18 pA/cm^2 and representative B, N, Mg, and O elemental maps taken during an intermediate irradiation stage. Electron irradiation may lead to moderate tube heating to an estimated temperature of 100−150 °C. First, we note that some dark-contrast precipitates appear during the initial heating stage, Figure 3b (some of them are barely visible in Figure 1a, albeit with bright-gray contrast, likely due to pretransformed domains; in fact, low dose irradiation is needed for an original HRTEM photo to be taken). Importantly, such dark-contrast regions were not peculiar to fresh, nonirradiated filling areas. Finally, a focused electron probe drills a hole in the filling, Figure 3c, due to complete melting and evaporation of the filled matter. More intense further irradiation heating leads to fragmentation of the filling and appearance of numerous voids in it, e.g., Figure 1c,d. The dark-contrast precipitate area is magnified in Figure 3d, where clear atomic fringes (or stacking faults) assigned to appearing second phase domains (most likely Mg-based solid solution in the present case) become visible. Such domains look relatively dark on a highly inhomogeneous spatially resolved O map, Figure 3h, in accord with the lack of oxygen in them, as compared to the O-rich MgO_2-based matrix. We also note the marked brightness variations of the O map along the filling in Figure 3h. Significant variations in the O content in irradiated MgO_2-based fillings are also effectively highlighted through taking O composition profiles across the filling (Figure 3h, inset). Conversely, the fully correlating B and N maps, and anti-correlating Mg map peculiar to the tube walls and the filled matter, respectively, are rather uniform, Figure 3e−g. Again no significant amounts of B and N are seen in the filling (the B and N maps are not sufficiently bright in the central part; rather they show the highest brightness in the tube walls); the results are in a good agreement with those obtained with the EELS and EDS techniques. Therefore all the experimental facts may be reasonably well interpreted in the sense that oxygen may be released from the MgO_2-based filling upon moderate heating; thus an O-poor Mg-containing phase, e.g., a stable MgO or Mg-based solid solution, should appear as a result of the oxygen outflow. It is also natural to suggest that the escape of O primarily takes place through the open tube ends, Figure 2a (inset).

Figure 4a−d shows the results of a detailed study of a regarded oxygen release from the MgO_2-based fillings. Parts a and b of Figure 4 compare two representative ED spectra (out of ~30 studied) taken on the as-prepared specimen composed of MgO_2-based filled BN nanotubes and the same specimen aged at room temperature over 2 months. The oxygen content dramatically drops from O/Mg ~ 2.0 (Figure 4a) to O/Mg ~ 1.0 (Figure 4b) atomic ratios. The latter composition matches a stable stoichiometric MgO oxide. Oxygen outflow was also observed on an individual BN-shielded MgO_2-based filling

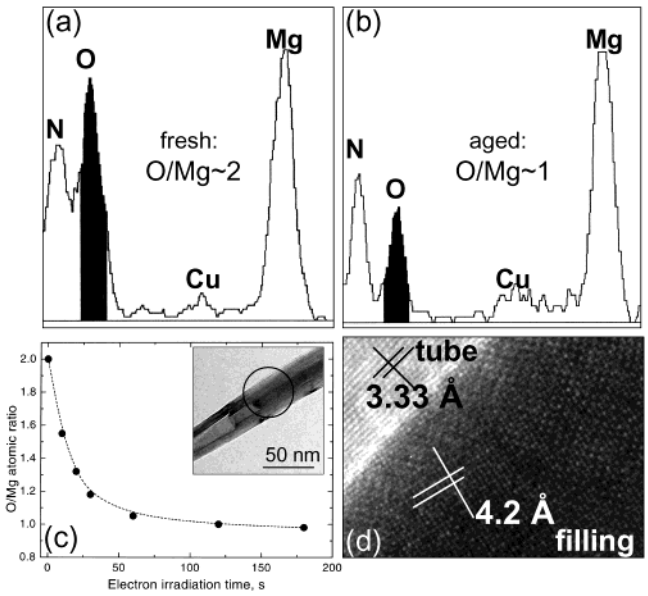

Figure 4. (a), (b) Representative comparative ED spectra consecutively taken on an as-prepared BN-shielded MgO_2-based-filled nanotube specimen and the same specimen aged over 2 months at room temperature, respectively. The O-peaks of interest are marked in black in the spectra. Note that the latter filling displays stable MgO composition. Cu peaks in the spectra solely originate from the TEM grid used. (c) A decay in the O-content in a given oxygen-rich filling (i.e., unstable MgO_2, displayed in the inset) as a function of the irradiation time with a ~5.7 pA/cm^2 current density; the O/Mg ratio quickly drops to ~1.0 (i.e., stable MgO) just within several tens of seconds and, then, does not notably change. (d) High-resolution TEM image of a filled BN nanotube aged at room temperature and viewed along the [001] zone axis of a fcc lattice peculiar to a filling matter. A measured lattice parameter of ~4.2 Å perfectly matches that of MgO. A 3.33 Å fringe separation natural for the (0002) shielding BN tubular layers is also shown.

during its electron beam heating, Figure 4c. A decay in oxygen content quickly proceeds just within several tens of seconds, again from O/Mg ~ 2.0 to O/Mg ~ 1.0 atomic ratios, and then, does not notably change. Finally, the sol presence of stable MgO-based fillings, rather than unstable MgO_2-based fillings in the specimens aged at room temperature was confirmed through high-resolution and electron diffraction work, Figure 4d. MgO is known to possess a face-centered-cubic (fcc) NaCl-type lattice with a lattice parameter of 4.2 Å.[21] A HRTEM image of the fragment of an aged BN tube-shielded filling is shown in Figure 4d. The image may be easily indexed as the NaCl lattice viewed along the [100] zone axis and exhibiting the (020) and (002) lattice fringes consistent with a 4.2 Å lattice parameter of the fcc structure.

To sum up, we were able to create MgO_2-based fillings inside chemically and thermally stable BN nanotubes. Under moderate heating and/or room temperature aging, the fillings easily decompose, leaving stable Mg-containing phases inside the tubes, while the oxygen may be locally generated from the nanotubes. Thus the first nanoscale oxygen burner/generator has become available.

Finally, let us suggest several intriguing practical applications of the observed phenomenon. Localized (several tens of nanometer pipe cross-section) oxygen outflow may selectively and effectively produce nanosize metallic domain oxidation. This may be applied in quantum dots preparation or local insulation of parts of a given conducting network composed of inorganic conducting nanowires. Study on various biological cell, bacteria, and/or individual molecule interaction with a point (nanometer size) oxygen source may shed light on their living and deteriorating conditions. This may be of high value in biological and medical science.

Acknowledgment. The present work was carried out in line with the "Nanoscale Materials" Project tenable at the National Institute for Materials Science, Tsukuba, Japan. We are grateful to Drs. R. Ma, F. Xu, Y. Li, and E. Kopnin for valuable discussions.

References and Notes

(1) Iijima, S. *Nature (London)* **1991**, *354*, 56.
(2) Dillon, A. C.; Jones, K. M.; Bekkedahl, T. A.; Kiang, C. H.; Bethune, D. S.; Heben, M. J. *Nature (London)* **1997**, *386*, 377.
(3) Liu, C.; Fan, Y.; Liu, M.; Cong, H. T.; Cheng, H. M.; Dresselhaus, M. S. *Science* **1999**, *286*, 1127.
(4) Trasobares, S.; Stephan, O.; Colliex, C.; Hug, G.; Hsu, W. K.; Kroto, H. W.; Walton, D. R. M. *Eur. Phys. J.* **2001**, *B22*, 117.
(5) Terrones, M.; Kamalakaran, R.; Seeger, T.; Ruhle, M. *Chem. Commun. (Cambridge)* **2000**, 23, 2335.
(6) Blase, X.; Rubio, A.; Louie, S. G.; Cohen, M. L. *Europhys. Lett.* **1994**, *28*, 335.
(7) Chopra, N. G.; Luyken, R. J.; Cherrey, K.; Crespi, V. H.; Cohen, M. L.; Louie, S. G.; Zettl, A. *Science* **1995**, *269*, 966.
(8) Golberg, D.; Bando, Y.; Kurashima, K.; Sato, T. *Scr. Mater*. **2001**, *44*, 1561.
(9) Samsonov, V. G. *The Oxide Handbook*; Plenum Press: New York, 1973; p 89.
(10) Massalski, T. *Binary Alloy Phase Diagrams*, 2nd ed.; ASM International: Vol. 3, p 2531.
(11) Konigstein, M.; Catlow, C. R. A. *J. Solid State Chem*. **1998**, *140*, 103.
(12) Titova, K. V.; Nikolskaya, V. P. *Russ. J. Inorg. Chem*. **2000**, *45*, 1331.
(13) Wang, Z. L.; Bentley, J.; Kenik, E. A.; Horton, L. L.; Mckee, R. A. *Surf. Sci.* **1992**, *273*, 88.
(14) Elprince, A. M.; Mohamed, W. H. *Soil Sci. Soc. Am. J.* **1992**, 56, 1784.
(15) Borden, R. C.; Goin, R. T.; Kao, C. M. *Cround Water Monitoring Remediation* **1997**, *17*, 70.
(16) Waite, A. J.; Bonner, J. S.; Autenrieth, R. *Environ. Eng. Sci.* **1999**, *16*, 187.
(17) Schmidtke, T.; White, D.; Woolard, C. J. *Hazardous Mater*. **1999**, *64*, 157.
(18) Gupta, B. K.; Glicklich, D.; Tellis, V. A. *Transplantation* **1999**, *67*, 1485.
(19) Tang, C. C.; Bando, Y.; Sato, T.; Kurashima, K. *Chem. Commun*. **2002**, 1290.
(20) Searcy A.; Meyers, C. E. *J. Phys. Chem.* **1957**, *61*, 957.
(21) Encyclopedia Britanica, Inc. 1994.